High-Efficiency High-Order *CL-LLC* DC/DC Converter With Wide Input Voltage Range

Xiangjun Zhang, *Member, IEEE*, Jiachen Jing, Yueshi Guan, *Member, IEEE*, Mingcong Dai, Yijie Wang, *Senior Member, IEEE*, and Dianguo Xu, *Fellow, IEEE*

***Abstract*—A novel multiresonant dc–dc converter is presented in this article, which owns a wide input voltage range and better voltage gain characteristics. Due to the addition of an antiresonant tank with a notch filter function, the converter introduces third harmonics in the power transmission, which can reduce the circulating energy in the resonant tank and reduce the loss of rectifier diode, thus improving the efficiency. The *CL–LLC* converter can realize soft switching in the full-load range. This article introduces the operating principle of the converter and the method of the parameters design. Finally, a 350–500 V input and 24 V/400-W prototype is designed to verify the correctness of the theory.**

***Index Terms*—DC–DC converter, high efficiency, higher order resonant tank, wide voltage range.**

I. Introduction

In RECENT years, with the development of power electronics technology, new energy technology has developed rapidly. However, photovoltaic, wind power, and other new energy generally have the disadvantage of unstable output. Therefore, it is of great significance to design a converter that can be applied to wide input conditions.

Resonant converters have been widely used [1]–[3]. An *LLC* converter can realize zero voltage switching (ZVS) for the primary-side and zero current switching (ZCS) for the secondary-side diode [1], so it is a preferred topology for small and medium power converters. According to its working principle, the voltage regulation can be realized by adjusting its switching frequency. However, its voltage regulation performance is poor when the frequency is larger than the resonant frequency, and the excessively wide switching frequency range is not conducive to the design of magnetic devices, so it cannot be used in applications with wide input voltage.

In order to solve the problem of high gain and high efficiency in a wide input range, scholars around the world have made a lot of exploration and research. According to the operation characteristics of resonant converter, there are three kinds of improvement methods. The first method is to change the amplitude of the basis wave on the input side, which includes the cutover of full-bridge and half-bridge topology, the duty cycle amplitude accompanying modulation [4], [5] after the introduction of multilevel, and the fixed-frequency phase-shifting control [6]. The second method is to change the resonant slot circuit structure, such as adding *LC* winding [7] and multiresonant slot [8]. The third method is to change the amplitude of the basis wave of the output side, including changing the turn ratio [9], changing the feedback voltage [10], and changing the rectification mode [11].

In order to achieve wide gain, a four-element *LCCL* multiresonant converter is proposed in [12]. The structure of a notch filter is introduced into the *LLC* resonant tank, and the fast attenuation characteristics of the notch filter are used to improve the high-frequency gain characteristics of *LLC*. It can be seen from the gain curve that the gain characteristics of the *LCCL* converter have been significantly improved. The gain decreases rapidly with the increase of frequency, and theoretically, the gain can be drop to 0. Therefore, wide gain adjustment can be realized with a narrow frequency range. However, the gain characteristics of an *LCCL* converter above the notch resonant frequency are not good enough, and the gain is greatly affected by the load, which is not conducive to the transmission of higher harmonics.

The method of utilizing harmonics to reduce the rms value of resonant current has been proposed in [13]. A simple passive auxiliary circuit is proposed. As a result, a minimum of 20% reduction in rms current is achieved to decrease the conduction losses in the power switches and in the auxiliary circuit. Also, a 65% reduction in switching frequency variation is obtained.

In order to further improve the performance of the converter, some five-element multiresonant converters topology is proposed in [14]–[16]. It is concluded that these converters can not only achieve wide gain but also transmit active power by high-order harmonics. Moreover, its structure and control mode are simple. Therefore, compared with the conventional wide gain converter, the converter has greater advantages. Compared with the five-element multiresonant topology proposed in [17], the advantages and parameters design of multiresonant converter are fully reflected in this article.

In this article, a multiresonant topology based on the *LLC* converter is proposed. The sensitivity of the voltage conversion ratio in the operating frequency range is improved by introducing a notch filter, and the third harmonic can be injected to

Manuscript received October 19, 2020; revised February 19, 2021; accepted March 11, 2021. Date of publication March 22, 2021; date of current version June 1, 2021. This work was supported in part by the National Natural Science Foundation of China under Grant 52007041, in part by the Power Electronics Science and Education Development Program of Delta Group under Grant DREG2020008, and in part by the Natural Science Foundation of Heilongjiang Province under Grant LH2020E050. Recommended for publication by Associate Editor A. Safaee. *(Corresponding author: Yueshi Guan.)*

The authors are with the School of Electrical Engineering and Automation, Harbin Institute of Technology, Harbin 150001, China (e-mail: xiangjunzh@hit.edu.cn; jingjiachenhit@163.com; guanyueshi@hit.edu.cn; 18s006071@hit.edu.cn; wangyijie@hit.edu.cn; xudiang@hit.edu.cn).

Color versions of one or more figures in this article are available at https://doi.org/10.1109/TPEL.2021.3067715.

Digital Object Identifier 10.1109/TPEL.2021.3067715

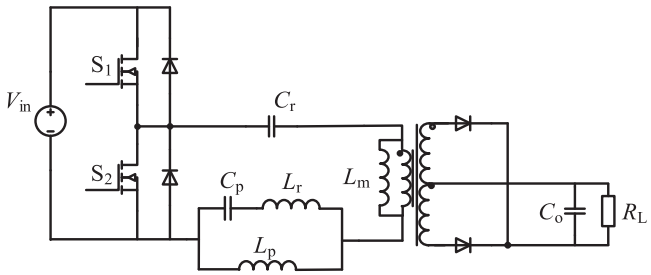

Fig. 1. *CL-LLC* resonant dc/dc converter.

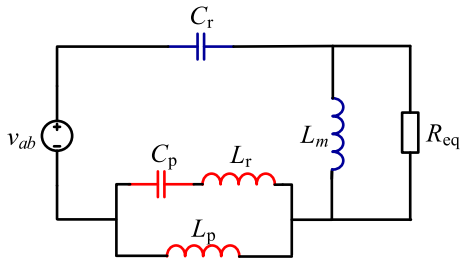

Fig. 2. Circuit diagram of the proposed converter.

transmit active power. Therefore, the wide range of input and the reduction of reactive power of the converter are realized simultaneously.

II. Operation of *CL-LLC* Converter

The proposed *CL-LLC* resonant dc/dc converter is shown in Fig. 1.

To simplify the analysis, the following assumptions are made for the circuit components.

1) The converter is in a stable running state.
2) The filter capacitance is large enough to ignore the output ripple voltage.
3) All inductors, capacitors, and transformers are ideal components. The equivalent series resistance (ESR) values of C_p, L_r, C_r, and L_p at the fundamental and third harmonics' frequencies can be ignored.

A. Characteristics Analysis

The *CL-LLC* converter was analyzed by fundamental harmonic analysis (FHA), and its simplified model was obtained, as shown in Fig. 2.

For resistive load, the following formula can be used to calculate the equivalent load on the primary side:

$$R_e = \frac{8n^2}{\pi^2}R. \tag{1}$$

When the converter operates at the resonant frequency, the impedance of the resonant tank is zero; thus

$$\frac{1}{j\omega C_r} + \left(\frac{1}{j\omega C_p} + j\omega L_r\right)//j\omega L_p = 0. \tag{2}$$

From (2), the expression of resonant frequency can be obtained as

$$f_{r1} = \sqrt{\frac{k+q+kq-\sqrt{(k+q+kq)^2-4kq}}{2kq}}f_{r0} \tag{3}$$

$$f_{r2} = \sqrt{\frac{k+q+kq+\sqrt{(k+q+kq)^2-4kq}}{2kq}}f_{r0}. \tag{4}$$

The parameters in the formulas above are defined as

$$k = \frac{L_p}{L_r}, \quad q = \frac{C_p}{C_r}, \quad f_{r0} = \frac{1}{2\pi\sqrt{L_rC_r}}. \tag{5}$$

In addition, when the C_p, L_r, and L_p of the notch filter resonant are given, the resonant frequency is expressed as follows:

$$f_{rp} = \sqrt{\frac{1}{q\,(k+1)}}f_{r0}. \tag{6}$$

Based on the FHA method, the transfer function expression of the *CL-LLC* converter can be obtained as

$$H(j\omega) = \frac{j\omega L_m//R_e}{\frac{1}{j\omega C_r} + (\frac{1}{j\omega C_p} + j\omega L_r)//j\omega L_p + j\omega L_m//R_e}. \tag{7}$$

The final transfer function can be simplified as (8), shown at the bottom of this page.

Take the model of (8), the system gain is obtained in (9), shown at the bottom of this page.

The parameters in (9) are defined as

$$Q = \frac{\sqrt{L_r/C_r}}{R_e}, \quad \lambda = \frac{L_r}{L_m}, \quad f_n = \frac{f_s}{f_{r1}}$$

$$\eta = \frac{f_{r1}}{f_{r0}} = \sqrt{\frac{k+q+kq-\sqrt{(k+q+kq)^2-4kq}}{2kq}}.$$

The gain curve of the multiresonant converter is shown in Fig. 3. Since the impedance characteristic of the multiresonant

$$H(j\omega) = -\frac{1}{j\frac{Q}{\eta f_n}\left[1+\frac{k\eta^2 {f_n}^2\left(q\eta^2 {f_n}^2-1\right)}{1-q\eta^2 {f_n}^2(1+k)}\right]+\left[\frac{\lambda}{\eta^2 {f_n}^2}\left(1+\frac{k\eta^2 {f_n}^2\left(q\eta^2 {f_n}^2-1\right)}{1-q\eta^2 {f_n}^2(1+k)}\right)\right]-1} \tag{8}$$

$$M\left(\lambda, f_n, Q\right) = \frac{1}{\sqrt{\left\{\left[\frac{\lambda}{\eta^2 {f_n}^2}\left(1+\frac{k\eta^2 {f_n}^2\left(q\eta^2 {f_n}^2-1\right)}{1-q\eta^2 {f_n}^2(1+k)}\right)\right]-1\right\}^2+\left\{\frac{Q}{\eta f_n}\left[1+\frac{k\eta^2 {f_n}^2\left(q\eta^2 {f_n}^2-1\right)}{1-q\eta^2 {f_n}^2(1+k)}\right]\right\}^2}} \tag{9}$$

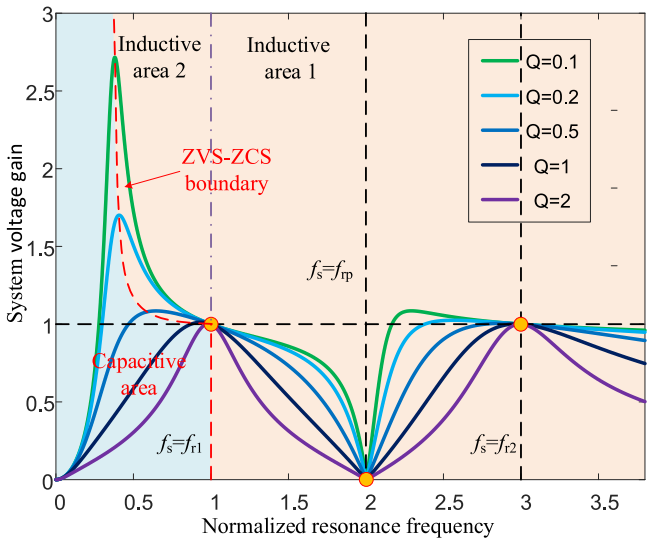

Fig. 3. Gain curve of the multiresonant converter.

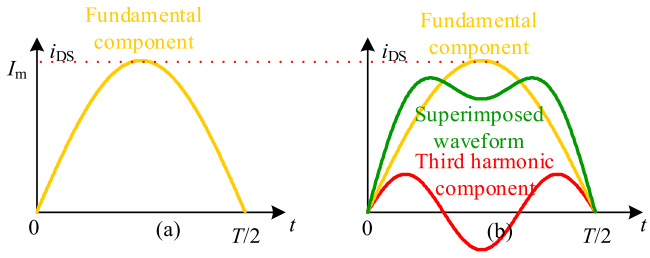

Fig. 4. *LLC* and *CL-LLC* diode rectified waveforms.

converter is basically the same as that of the *LLC* converter, the gain characteristic of the multiresonant converter is similar to that of the conventional *LLC* converter. In $f_{r1} < f_s < f_{rp}$, the gain of the multiresonant converter decreases significantly with the increase of frequency due to the addition of the notch filter, which means that the dc gain has a large response amplitude to the frequency change. This is because the infinite impedance generated by the parallel resonance of C_p, L_r, and L_p can reduce the gain of the multiresonant converter to zero. According to the characteristic that the gain can be reduced to zero, it is feasible to realize the inherent soft-start capability and overcurrent protection function of the multiresonant converter by controlling the switching frequency.

It can be seen from the gain curve that *CL-LLC* has better voltage regulation characteristics. Compared with the traditional *LLC* converter, the multiresonant converter has obvious advantages in the gain adjustment range. At the same time, we can find that the gain characteristics of the *CL-LLC* converter are similar to two bandpass filters, which can transfer the fundamental and higher harmonics simultaneously.

Considering that the third harmonic is the highest harmonic in the input square-wave voltage, the third harmonic can be used to transfer power and reduce reactive power circulation.

The comparison of transmission power between *CL-LLC* and *LLC* is shown in Fig. 4.

When the *LLC* converter works at a resonant frequency, the current is completely sinusoidal and can only utilize the fundamental wave to transmit active power; for the *CL-LLC* converter, the current takes the shape of a saddle wave, and the third harmonic is injected to transfer active power. According to the Fourier decomposition, in the square-wave voltage input to the resonator, the content of the third harmonic is one-third of the fundamental wave. Therefore, at the resonant point for the resonant current, the content of the third harmonic current is also about one-third of the fundamental wave current. In this way, 10% of the active power can be transmitted theoretically through the third harmonic.

If the peak value of the fundamental sine wave is assumed I_m, the calculations of the half-wave sine mean value and effective value are as follows:

$$\overline{I} = \frac{1}{2\pi}\int_0^{\pi} I_m \sin\omega t d\omega t = \frac{I_m}{\pi} \tag{10}$$

$$I_{(\mathrm{rms})} = \sqrt{\frac{1}{2\pi}\int_0^{\pi} (I_m \sin\omega t)^2 d\omega t} = \frac{I_m}{2}. \tag{11}$$

The average value and effective value of the saddle waveform with the third harmonic injection are calculated as follows:

$$\overline{I^*} = \frac{1}{2\pi}\int_0^{\pi} I_m(\sin\omega t + \frac{1}{3}\sin 3\omega t) d\omega t = \frac{\sqrt{10}}{6} I_m \tag{12}$$

$$I^*_{(rms)} = \sqrt{\frac{1}{2\pi}\int_0^{\pi} \left(I_m \sin\omega t + \frac{1}{3} I_m \sin 3\omega t\right)^2 d\omega t} = \frac{10 I_m}{9}. \tag{13}$$

Compared with the ordinary half-wave sinusoidal current, the effective value of the saddle waveform increased by 2.22 times and the average value increased by 1.65 times. Under the condition of the same power with the same effective value, the average value of the current with the third harmonic injection can be reduced to 26%.

B. Operation Principles

The main working waveform is shown in Fig. 5, i_{Lr} is the current of the resonant inductor, and i_{Lm} is the current of the magnetizing inductance. i_{D1} and i_{D2} are, respectively, the currents of the rectifier diodes D_1 and D_2.

Since there are many working modes in this subject, we take working modes in $f_{r1} < f_s < f_{rp}$ as an example and introduce the operating modes in this frequency band. The equivalent circuits of different stages are shown in Fig. 6. The operation of each working mode is described as follows.

1) STAGE I $[t_0, t_1]$: At t_0, the switch performs the shutdown operation and the resonant converter enters the dead-time. Resonant current charges S_1 until its body diode is switched ON at which point S_1 is driven and the soft switching is achieved. During this period, the resonant energy will be transmitted back to the input end. At the time of t_1, the resonant current reaches zero.
2) STAGE II $[t_1, t_2]$: In the time of $[t_1, t_2]$, the S_1 is driven. At this time, the magnetic inductance is still being clamped

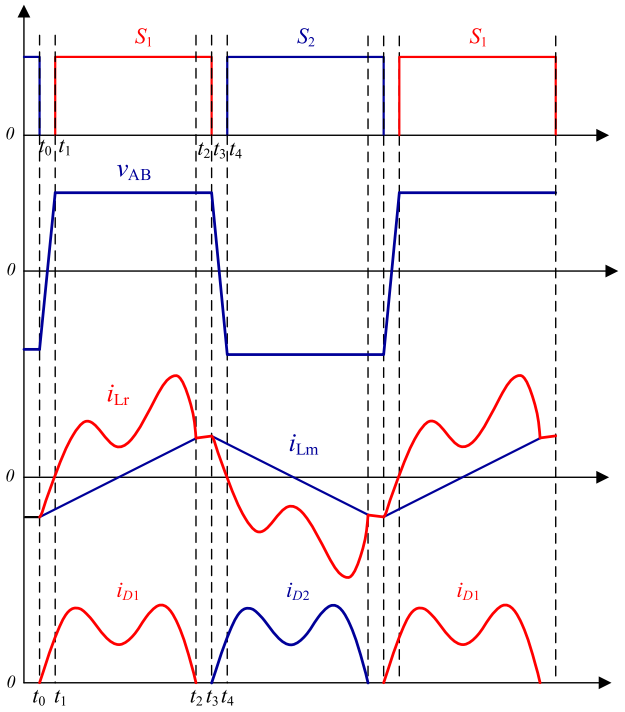

Fig. 5. Key working waveforms of the converter in $f_{r1} < f_s < f_{rp}$.

by the output voltage, and the energy transmits from the input end to the output end through the transformer. At t_2, the resonant current is equal to the magnetic current.

3) STAGE III [t_2, t_3]: At t_2, the load energy comes from the energy storage capacitor of the output end, and the transformer cannot transmit energy at this time.
4) STAGE IV [t_3, t_4]: At t_3, S_1 and S_2 are both not driven, and the system enters the deadtime again. The parasitic capacitance of switches is charging or discharging. The body diode of the switch is ON, which provides a condition for soft switching. At time t_4, deadtime ends and the system enters the second half-cycle.

The working process of the second half-cycle is similar and no longer repeated.

III. Design Procedure of Circuit Parameters

In this chapter, we analyze the effect of key resonant network parameters, and the scheme of parameter design from the angle of optimal efficiency is summarized. Finally, a 400-W prototype is taken as an example to give the design process of resonator parameters.

A. Principles of Parameters Design

The *CL-LLC* converter has five resonant components, respectively, L_m, L_r, C_r, L_p, and C_p. Before designing resonant network parameters, it is necessary to analyze the influence of these resonant elements on the converter. Based on (1), (3), (4), and (9), the parameters can be calculated as

$$L_r = \frac{QR_e}{2\pi f_{r0}} \tag{14}$$

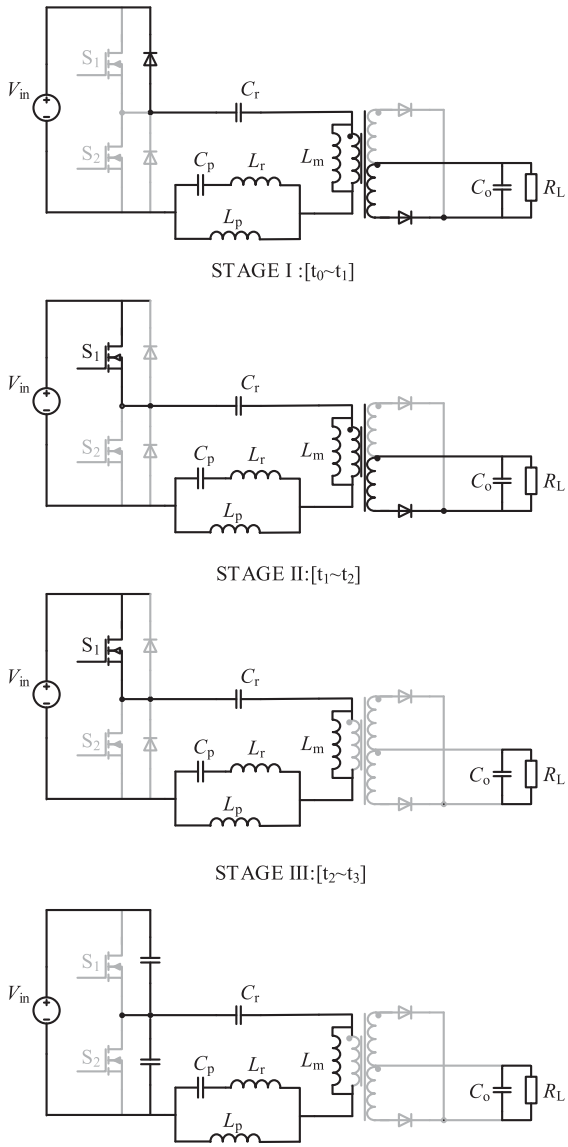

Fig. 6. Equivalent circuits of different stages: Stage I: [t_0, t_1], Stage II: [t_1, t_2], Stage III: [t_2, t_3], and Stage IV: [t_3, t_4].

$$C_r = \frac{1}{2\pi f_{r0} Q R_e} \tag{15}$$

$$L_m = \frac{L_r}{\lambda} \tag{16}$$

$$L_p = kL_r \tag{17}$$

$$C_p = qC_r. \tag{18}$$

R_e and f_{r0}, respectively, represent the ac equivalent resistance and series resonant frequency. R_e is determined by the performance index, and f_{r0} can be selected by the switching frequency during the design. It can be seen from (14)–(18) that the parameters of the five resonant elements are actually only related to k, q, λ, and Q.

Generally speaking, the loss of MOSFET mainly includes the conduction loss and switching loss. Since the resonant converter

can realize ZVS, there is no turn-ON loss, so the switching loss only considers the turn-OFF loss. The conduction loss and turn-OFF loss are directly related to resonant current $I_{Lr(rms)}$ and magnetic inductance current $I_{Lm(\max)}$. Therefore, the influence of resonant element parameters on $I_{Lr(rms)}$ and $I_{Lm(\max)}$ is mainly analyzed in the loss analysis.

To simplify the analysis, the converter is assumed to operate at resonant frequency points. At this point, the fundamental wave and the third harmonic gain are 1, and the cavity impedance is zero. Assuming that the magnetic inductance is large enough, the fundamental wave presents the same impedance as the third harmonic, and the resonant current can be expressed as

$$i_{Lr}(t) = \sqrt{2} I_{Lr} \sin(\omega_r t + \varphi) + \frac{\sqrt{2}}{3} I_{Lr} \sin(3\omega_r t + \varphi). \quad (19)$$

In (19), I_{Lr} represents the effective value of the resonant current, while φ represents the phase difference between the fundamental wave voltage and current.

As the magnetic inductance is clamped by the output voltage, the current waveform changes linearly, which can be expressed as follows:

$$I_{Lm}(t) = \begin{cases} \frac{nV_o}{L_m}(t - \frac{T}{4}) & 0 \le t < \frac{T}{2} \\ \frac{nV_o}{L_m}(\frac{3T}{4} - t) & \frac{T}{2} \le t < T. \end{cases} \quad (20)$$

In (20), T is the resonant period, and n is the turn ratio of the transformer.

According to the initial value of resonant current and magnetic inductance current equals each other, it can be obtained as follows:

$$I_{Lr}(t_0) = \frac{4\sqrt{2}}{3} I_r \sin\varphi = -\frac{nV_0 T}{4L_m}. \quad (21)$$

From (19)–(21), the following can be solved:

$$I_{Lr}(rms) = \frac{3nV_0}{4R_e} \sqrt{\frac{{R_e}^2 {T_r}^2}{32{L_m}^2} + \frac{9}{50}\pi^2} \quad (22)$$

$$I_{Lm}(\max) = \frac{nV_0 T}{4L_m}. \quad (23)$$

In order to make the analysis general, it is necessary to normalize the current. Current reference I_N is defined as follows:

$$I_N = \frac{nV_0}{R_e}. \quad (24)$$

The L_m expression in (16) is substituted into (22) and (23) and normalized in accordance with (24), and the following equation can be obtained as:

$${I_{Lr}}^*(\mathrm{rms}) = \frac{I_{Lr}(\mathrm{rms})}{I_N} = \frac{3\pi}{4} \sqrt{\frac{\lambda^2}{8Q^2 \times \eta^2} + \frac{9}{50}} \quad (25)$$

$${I_{Lm}}^*(\max) = \frac{I_{Lm}(\max)}{I_N} = \frac{\pi\lambda}{2Q \times \eta}. \quad (26)$$

From the above analysis, it can be seen that the influence of resonant element parameters on the converter loss can finally be reduced to the influence of ${I_{Lr}}^*(\mathrm{rms})$ and ${I_{Lm}}^*(\max)$.

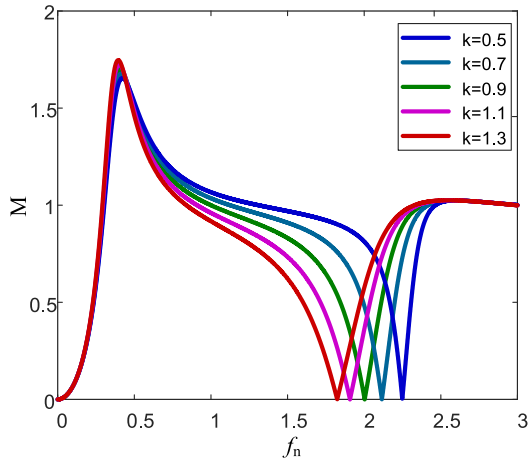

Fig. 7. Influence of k on converter gain ($q = 0.14$, $\lambda = 0.14$, and $Q = 0.4$).

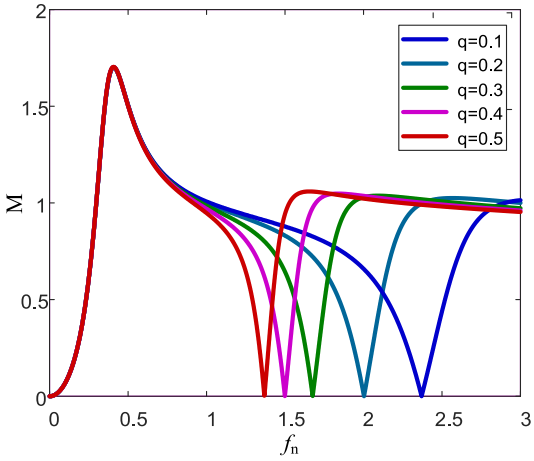

Fig. 8. Influence of q on converter gain ($k = 0.94$, $\lambda = 0.14$, and $Q = 0.4$).

B. Resonant Frequency Matching

It can be seen from the current expression that ${I_{Lr}}^*(\mathrm{rms})$ and ${I_{Lm}}^*(\max)$ are not directly related to the value of k and q. Therefore, the design of k and q is mainly considered from the perspective of the third harmonic utilization, and the influence on the current is not analyzed.

When k or q is changed, respectively, the gain curve changes, as shown in Figs. 7 and 8. It can be seen from the figure that the change of k and q will affect the position where the gain is zero, so as to determine the rate of descent of the gain curve above the resonant frequency, while it has almost no influence on the gain below the resonant frequency. This is because k and q directly affect the resonant frequency of the notch filter, and the introduction of the notch filter only affects the gain characteristics above the resonant frequency point.

According to the analysis above, the *CL-LLC* converter has three resonant frequency points f_{r1}, f_{r2}, and f_{rp} of the notch filter. Reasonable matching of these three resonant frequencies has an important effect on the converter.

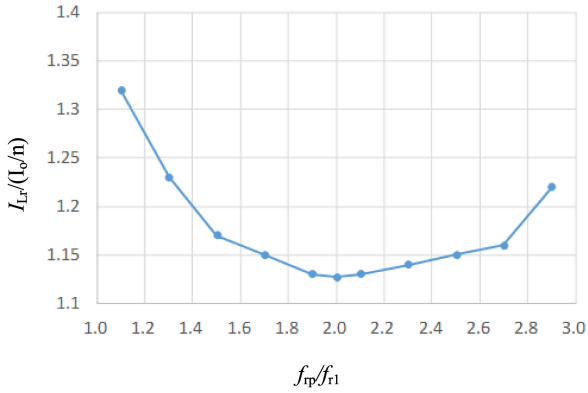

Fig. 9. Relation curve between the value of resonant current $I_{Lr}/(I_o/n)$ and f_{rp}.

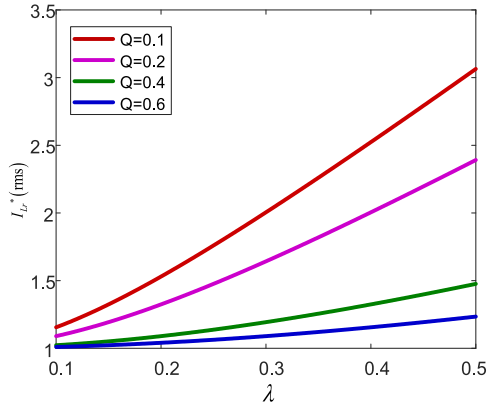

Fig. 10. Influence of λ and Q on the current $I_{Lm}{}^*(\max)$ ($q = 0.14$ and $k = 0.94$).

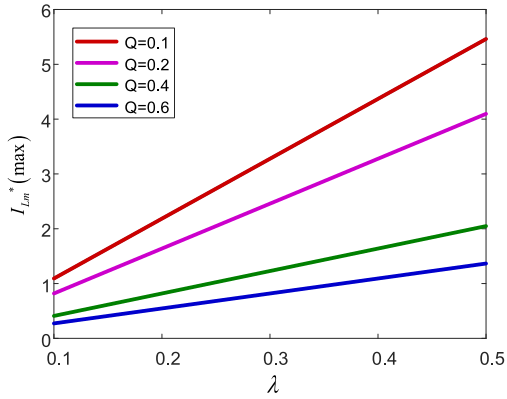

Fig. 11. Influence of λ and Q on the current $I_{Lm}{}^*(\max)$ ($q = 0.14$ and $k = 0.94$).

According to the Fourier analysis, the third harmonic is the highest harmonic in the input square-wave voltage. In order to make full use of the third harmonic, it is hoped that f_{r2} is set as $3f_{r1}$.

Since the notch filter is introduced to improve the gain characteristics when the switching frequency is higher than the first resonant frequency f_{r1}, f_{rp} should be higher than the first resonant frequency f_{r1}. At the same time, in order not to affect the third harmonic transmission, f_{rp} should be lower than the second resonant frequency f_{r2}. Thus, $f_{r1} < f_{rp} < f_{r2}$. However, f_{rp} cannot get too close to f_{r2}, which means the utilization rate of the third harmonic is greatly reduced. Similarly, f_{rp} cannot be too close to f_{r1}; otherwise, the fundamental wave transmission will be affected.

The substandard resonant current $I_{Lr}/(I_o/n)$ with different values of f_{rp} was analyzed by simulation, as shown in Fig. 9. As we can see, as the value of f_{rp} increases, $I_{Lr}/(I_o/n)$ decreases first and then increases. When $f_{rp} = (1.5\text{–}2.5)\, f_{r1}$, the resonant current is relatively low.

In addition, since the input square-wave voltage does not contain even harmonics, it is a good choice to set f_{rp} as $2\,f_{r1}$, which can reduce the loss of reactive power in the resonant tank.

If we set f_{r1} as 500 kHz, f_{r2} and f_{rp} can be designed as

$$f_{r2} = 3f_{r1} = 1.5\,\mathrm{MHz} \tag{27}$$

$$f_{rp} = 2f_{r1} = 1\,\mathrm{MHz}. \tag{28}$$

Combined with (27) and (28), the following equation can be solved as:

$$\begin{cases} k = \dfrac{L_p}{L_r} = 0.94 \\ q = \dfrac{C_p}{C_r} = 0.14 \\ \eta = \sqrt{\dfrac{k+q+kq-\sqrt{(k+q+kq)^2-4kq}}{2kq}} = 0.96 \\ f_{r0} = \dfrac{f_{r1}}{\eta} = 520.8. \end{cases} \tag{29}$$

C. Influence of Q and λ

According to (25) and (26), the curves of $I_{Lr}{}^*(\mathrm{rms})$ and $I_{Lm}{}^*(\max)$ varying with λ and Q can be drawn. Figs. 10 and 11 show that $I_{Lr}{}^*(\mathrm{rms})$ and $I_{Lm}{}^*(\max)$ both increase with the increase of λ, and the influence of λ is more obvious when Q is decreasing. As a result, the conduction loss and the switching loss of the converter will increase. So, from the perspective of efficiency, λ is desirable to be as small as possible.

It can be seen from Figs. 10 and 11 that, with the same λ, $I_{Lr}{}^*(\mathrm{rms})$ and $I_{Lm}{}^*(\max)$ will both decrease with the increase of Q, and the conduction loss and switching loss will also decrease. Therefore, from the perspective of efficiency, Q is desirable to be as large as possible.

The variation trend of the gain with respect to Q is shown in Fig. 12. It can be seen from the figure that with the increase of Q, the peak gain of the converter will decrease, which may cause the output voltage to fail to reach the required value. In terms of gain characteristics, Q is required to be as small as possible.

The gain curve of the *CL-LLC* converter with different λ is shown in Fig. 13. As we can see, with the decrease of λ, the peak gain decreases and the gain curve flattens out, which is not conducive to the design of a wide range of converters. In terms of gain characteristics, λ is required to be as large as possible.

D. Gain Constraints

The gain range is a key factor in resonant network parameters design. From the point of view of design, it is required that the gain range of the converter is larger than the actual gain range. It can be seen from the gain curve that the gain decreases

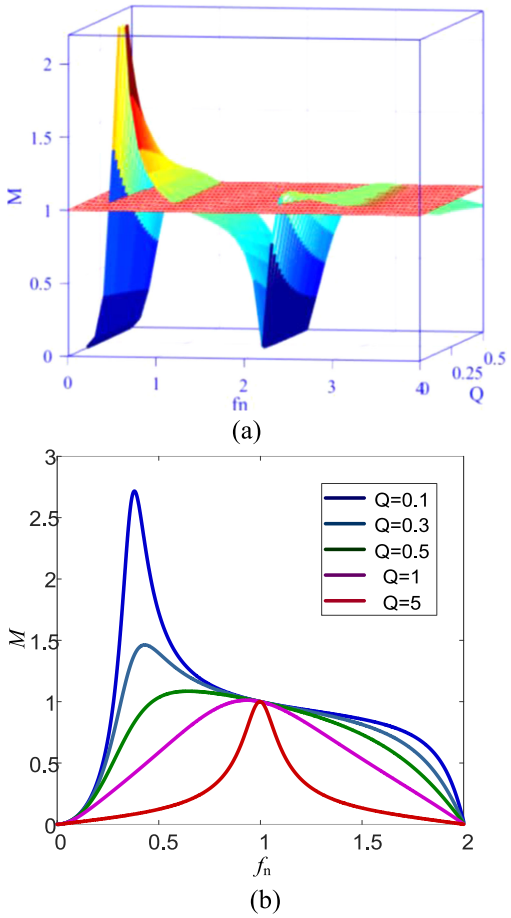

Fig. 12. Influence of Q on the gain of the converter ($q = 0.14$, $k = 0.94$, and $\lambda = 0.14$).

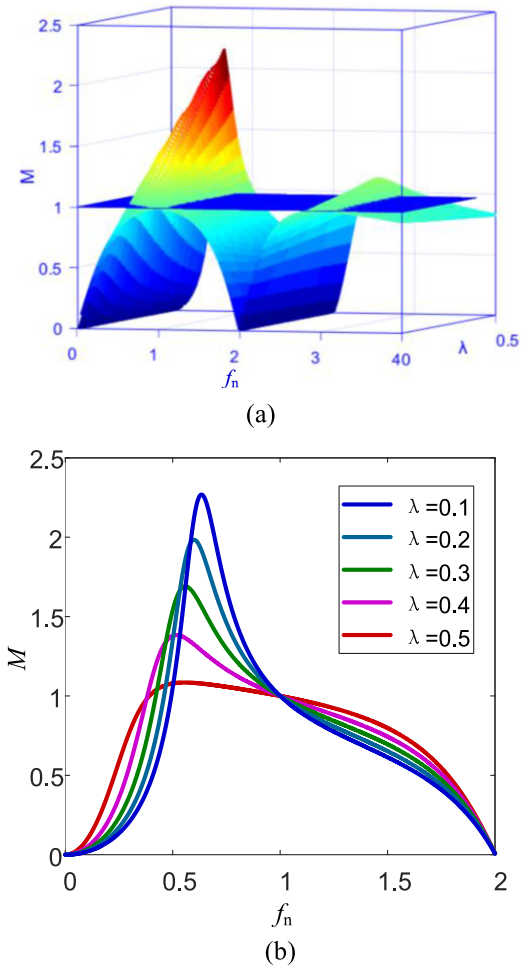

Fig. 13. Influence of λ on the gain of the converter ($q = 0.14$ and $k = 0.94$).

monotonically with the increase of frequency in the working frequency range. The gain varies with different loads. In the case of the same switching frequency, the gain of the light load is higher than that of heavy load and reaches the maximum under no-load condition. Take the wide output converter as an example, if the minimum output voltage with no-load and maximum output voltage with full-load can meet the gain requirement, then the converter can meet the gain requirement in the whole operating range. Therefore, the parameter design of *CL-LLC* should meet two criteria: the minimum output voltage gain under no-load condition should be low enough and the maximum output voltage gain with full-load is high enough.

1) The operating range that meets the minimum gain requirement.

Under the no-load condition, $Q = 0$ is substituted into the gain expression (9), and the following equation can be obtained:

$$M(\lambda, f_n) = \frac{1}{\left[\frac{\lambda}{\eta^2 {f_n}^2}\left(1 + \frac{k\eta^2 {f_n}^2 (q\eta^2 {f_n}^2 - 1)}{1 - q\eta^2 {f_n}^2 (1+k)}\right)\right] - 1}. \quad (30)$$

According to the previous analysis, when the resonant frequency matching is determined, the magnitude of k and q can be uniquely determined, and then M is only related to λ and f_n.

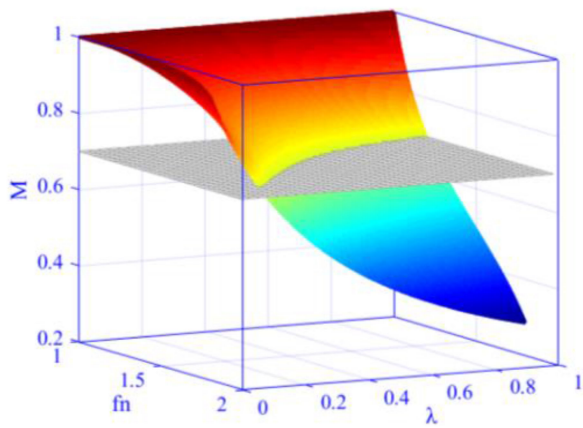

Fig. 14. Influence of λ and f_n on the voltage conversion ratio M and the minimum gain $M_{\min}$.

In order to meet the minimum gain $M_{\min}$ requirement of the converter, the gain at the highest frequency should be

$$M(f_{n\_max}) \leq M_{min}. \quad (31)$$

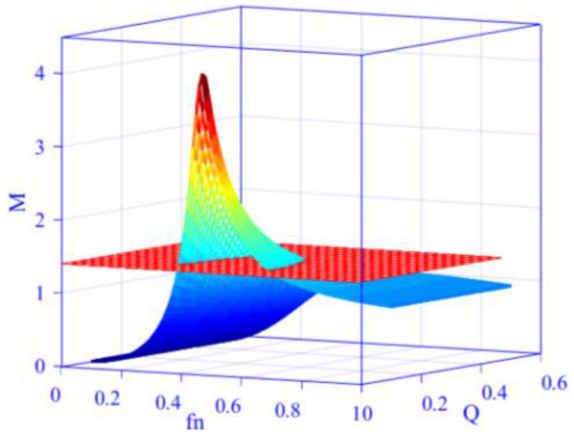

Fig. 15. Influence of Q and f_n on the voltage conversion ratio M and the maximum gain $M_{\max}$.

Fig. 14 shows the no-load gain surface with different λ and f_n and the $M_{\min}$ plane of minimum gain requirement. Obviously, the part below the plane meets the requirements. By projecting this part of the surface onto f_n and λ plane, the value range of λ and f_n can be obtained, which meets the minimum gain requirement. On the premise that the gain requirement is satisfied, the value of λ is desired to be as small as possible, which means the loss is minimized. λ is taken as 0.14.

2) The operating area that meets the peak gain requirement.

When λ is determined under the minimum gain requirement, the peak gain is only related to f_n and Q. In order to meet the maximum gain demand of the converter, the gain at the lowest frequency needs to satisfy

$$M\left(f_{n\_\min}\right) \geq M_{max}. \tag{32}$$

The influence of f_n and Q on the gain and the plane graph of peak gain $M_{\max}$ are shown in Fig. 15. The part above the $M_{\max}$ plane can meet the peak gain requirement. Similarly, by projecting this part of the surface onto the f_n and Q planes, the range of f_n and Q can be obtained where the peak gain requirement is satisfied. On the boundary line of the projected area, there exists a maximum value of Q, which is the optimal value of the design. As a result, Q is taken as 0.4.

According to (14)–(18), when k, q, λ, and Q are known, five resonance parameters L_r, C_r, L_p, C_p, and L_m can be calculated. The final step is to verify if the *CL-LLC* converter can implement the soft switching within the full-load range. If not, select Q and λ again until the soft switching is realized.

On the basis of the proposed parameter design method, the design process of the multiresonant converter is shown in Fig. 16.

IV. Experimental Results

According to the results of the previous design, a 400-W prototype platform was built to verify the feasibility of the proposed converter.

The electrical specifications are set as: $V_{\text{in}} = 350$—500 V, $V_{\text{out}} = 24$ V, and $P_{\text{out}} = 400$ W. The parameters obtained by obvious calculation are given in Table I. The digital control is

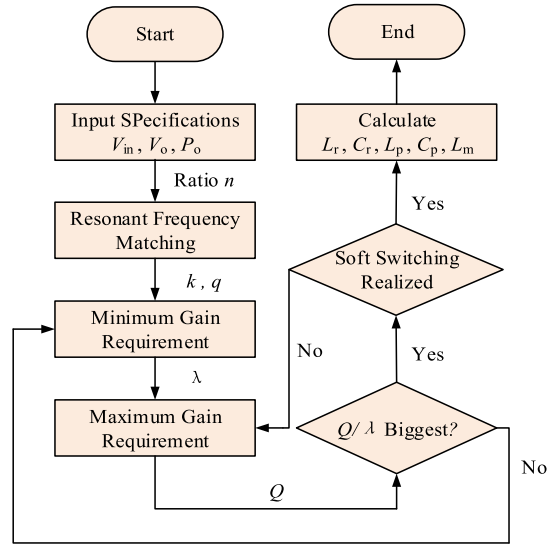

Fig. 16. Process of parameters design of the multiresonant converter.

TABLE I
Selected Parameters and Specifications of the Converter

Component	Specifications
MOSFETs	C2M0280120D
D_1, D_2	D2065C6
Driving chip	1EDI20N12AF
Switching Frequency	400kHz-660kHz
Turn ratio	8:1:1
L_{m}	33μH(core：EQ30)
L_r	6.7μH (core：EQ20)
C_{r}	13.9nF
L_p	6.3μH (core：EQ20)
C_p	1.95nF
C_{01}, C_{02}	100uF

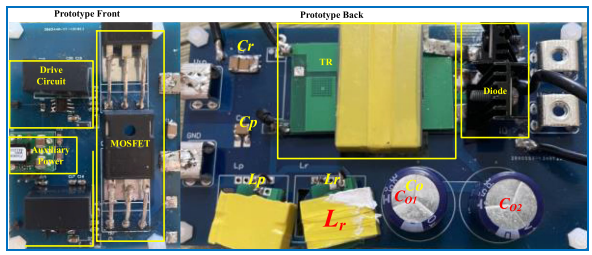

Fig. 17. Prototype of the proposed converter.

adopted, and the control chip is TMS320F28335. Fig. 17 shows the prototype of the proposed converter.

Figs. 18–20 show the steady-state experimental waveforms of different input voltages under different loads, where V_{gs} is the primary-side switch driving voltage, V_{ds} is the drain–source voltage, and i_r is the resonant current. As can be seen from the figures, the experimental results are basically consistent with the theoretical analysis. The primary-side switch can realize ZVS soft switching characteristic. Due to the injection of the third harmonic, the current waveform i_r changes in saddle-wave shape.

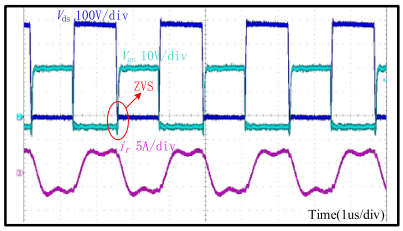

(a)

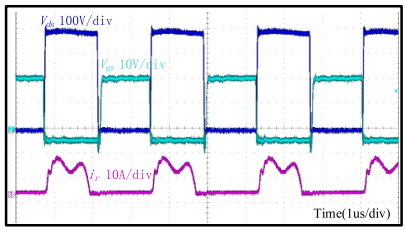

(b)

Fig. 18. Observed waveforms of the proposed converter at $V_{\text{in}} = 400$ V, $V_o = 24$ V, $P_o = 400$ W, and $f_s = 500$ kHz. (a) Primary-side working waveform. (b) Secondary-side working waveform.

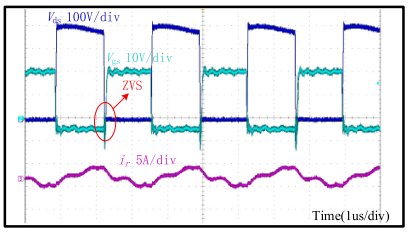

(a)

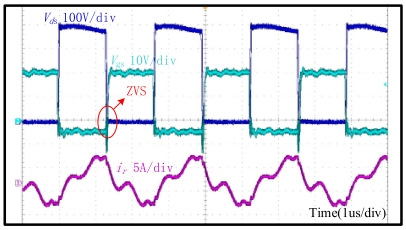

(b)

Fig. 19. Observed waveforms of the proposed converter at $V_{\text{in}} = 350$ V, $V_o = 24$ V, and $f_s = 400$ kHz. (a) Half-load working waveform, $P_o = 200$ W. (b) Full-load working waveform, $P_{\text{o}} = 400$ W.

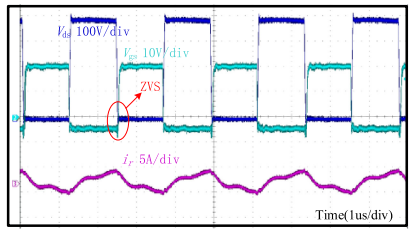

(a)

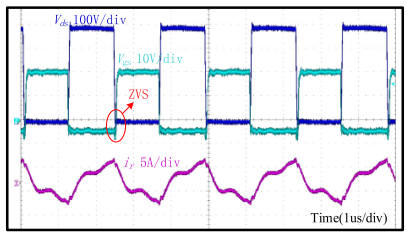

(b)

Fig. 20. Observed waveforms of the proposed converter at $V_{\text{in}} = 500$ V, $V_o = 24$ V, and $f_s = 660$ kHz. (a) Half-load working waveform, $P_o = 200$ W. (b) Full-load working waveform, $P_o = 400$ W.

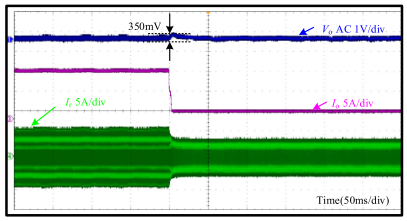

Fig. 21. Experimental waveforms of dynamic response.

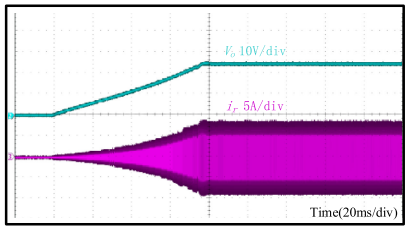

Fig. 22. Soft-start current and voltage waveform.

When the converter works exactly at the resonant frequency of 500 kHz, the gain of the third harmonic is also 1, and the injection of the third harmonic is more obvious.

In summary, the *CL-LLC* resonant converter proposed in this article can achieve soft switching within the full-load range.

Fig. 21 shows the dynamic response waveforms of the proposed converter. As we can see, the output voltage ripple is 350 mV, when I_o varies from 12 to 2 A, which takes 18 ms.

The experimental waveforms at soft start are shown in Fig. 22. Due to its gain characteristics, the switching frequency of the startup is set at the resonant frequency of the notch filter ($f_s = f_{rp}$). The switching frequency gradually decreases, and the output voltage finally reaches the closed-loop steady-state value.

Fig. 23 shows the short-circuit steady-state waveform. As can be seen, there is no high-current spike at the moment of the short circuit. By increasing the switching frequency to the notch resonant frequency, the current of the resonator is well limited. It can be seen that the proposed converter has good short-circuit protection ability.

The comparison of five multiresonant topologies for wide gain applications is given in Table II. It can be seen from Table II that the proposed topology has a significant advantage in efficiency. Compared with other topologies, the proposed converter can satisfy a wide gain while maintaining high efficiency. In addition,

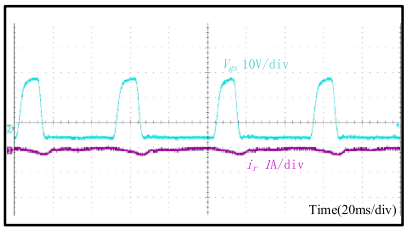

Fig. 23. Short-circuit experimental waveform.

TABLE II
COMPARISON OF THE PROPOSED CONVERTER WITH REFERENCES [18]–[21]

Topology	Frequency range	Voltage range	System Gain M	Efficiency
LC-LC [18]	110kHz~200kHz	330V~390V	1-1.2	95.0%
LCLC [19]	170kHz~260kHz	250V-400V	1.1-1.7	95.3%
LLC-LC [20]	44kHz~131kHz	132V~264V	0.6-1.2	95.1%
LCLCL [21]	74kHz~141kHz	50V~250V	0.3-1.4	96.3%
Proposed	400kHz~660kHz	350V-500V	0.9-1.3	95.9%

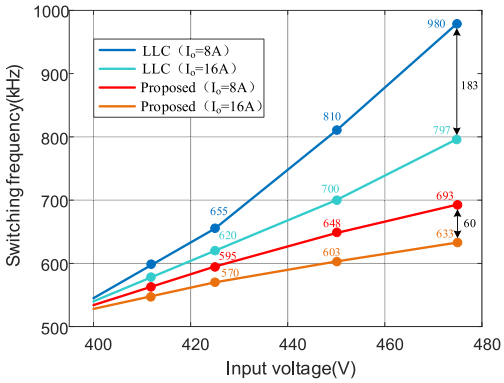

Fig. 24. Comparison of the switching frequency between *LLC* and the proposed converters at high-voltage input and at different loads.

under the same voltage variation, the frequency range of this topology is relatively narrow, making it easier to control and improve efficiency.

Fig. 24 shows the comparison of the switching frequency between *LLC* and *CL-LLC* converters at high-voltage input and at different loads. When the input voltage is very high, the switching frequency of *LLC* has to increase a lot, which means low efficiency. Compared with the *LLC* converter, the switching frequency range of the proposed converter is narrower. At $V_{\text{in}} = 475$ V, from full-load to half-load, the frequency of the *LLC* converter increases by 183 kHz, but the proposed converter only increases by 60 kHz.

Fig. 25 shows the efficiency comparison curves of the proposed *CL-LLC* converter and the traditional *LLC* converter under different input voltages, which are obtained under the same conditions. It can be seen from Fig. 25 that the efficiency of *LLC* and the proposed topology is not significantly different near the resonant frequency point. In the case of high input voltage, compared with the traditional *LLC* converter, the *CL-LLC* converter has obvious advantages in efficiency.

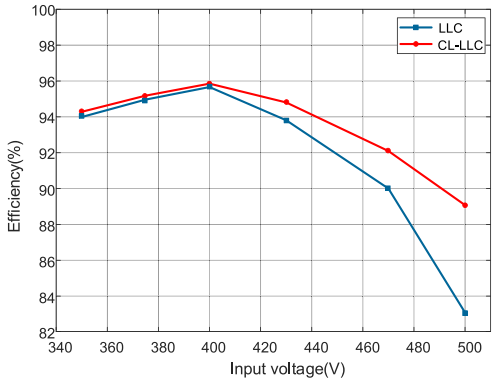

Fig. 25. Comparison of the efficiency between *LLC* and the proposed converter at different input voltages.

The power loss of the proposed converter contains the switching loss and conduction loss of the switch, inductor loss, diode loss, as well as the capacitor loss.

Inductor loss is divided into magnetic loss and copper loss as follows:

$$P_{\text{mag}} = P_V V_{\text{core}} \tag{33}$$

$$P_{\text{cop}} = {I_{\text{rms}}}^2 R_{\text{ac}}. \tag{34}$$

I_{rms} is the effective value of the current flowing through the winding. R_{ac} is the ac resistance at the corresponding frequency of the winding.

The conduction loss of the switch can be obtained as follows:

$$P_{\text{cond}} = I_s^2 R_{DS\text{on}} \tag{35}$$

where $R_{DS\text{on}}$ is the ON-state resistance of the switch. The value of the switch in this article is 280 mΩ. The switching loss can be calculated by the formula as follows:

$$P_{\text{off}} = \frac{V_{ds} I_{\text{off}} t_{\text{off}}}{6T} \tag{36}$$

where t_{off} is the time of the turn-OFF transition, which is 45 ns. V_{ds} represents the voltage across the switch. I_{off} is the value of the turn-OFF current.

The diode loss can be calculated by

$$P_{\text{diode}} = U_{D0} I_D. \tag{37}$$

Where, U_{D0} is the diode forward conduction voltage, and I_D represents the current flowing through the diode.

The loss of the resonant capacitor can be expressed as

$$P_{\text{c}} = R_{\text{ESR}} {I_c}^2 \tag{38}$$

where R_{ESR} and I_c represent the equivalent series resistor of the capacitor and the rms of the capacitor current, respectively.

Fig. 26 shows the power loss of the different elements of the proposed converter. Under the condition of full-load, at rated output, the total loss of the MOSFET is 4.8 W, the loss of the resonant capacitor is 1.2 W, the loss of the diode is 6.5 W, the loss of the inductor is 2.6 W, and the other loss is 1.2 W.

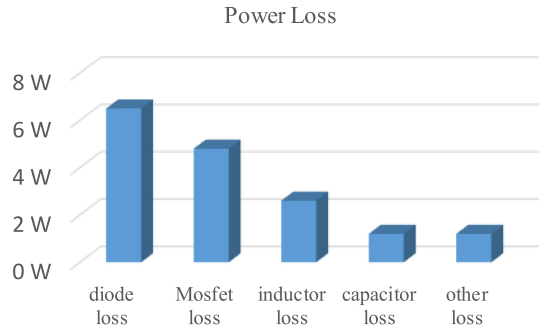

Fig. 26. Power loss of the different parts of the proposed converter.

V. Conclusion

In this article, a wide gain and high-efficiency multiresonant converter has been studied. By improving the *LLC* resonant tank and introducing the notch filter, a new five-element *CL-LLC* multiresonant converter is proposed. The operating principle and gain characteristics of the converter are analyzed in detail. It is indicated that the topology is suitable for the wide range of voltage input or output applications. At the same time, the multiresonant converter can realize soft switching over the entire working range, which can ensure high efficiency of the converter. Compared with the conventional *LLC* converter, this converter has the advantage of the third harmonic being introduced for energy transmission. In this article, a 400-W prototype is designed. The experimental results verify the correctness of the theoretical analysis and parameter design

References

[1] H. Guisong *et al.*, "Half-bridge LLC series resonant converter," Delta Power Electron. Center, Shanghai, China, 2000.
[2] Y. Guan, C. Liu, Y. Wang, W. Wang, and D. Xu, "Analytical derivation and design of 20-MHz DC–DC soft-switching resonant converter," *IEEE Trans. Ind. Electron.*, vol. 68, no. 1, pp. 210–221, Jan. 2021.
[3] Y. Guan, Y. Wang, W. Wang, and D. Xu, "A 20 MHz low-profile DC–DC converter with magnetic-free characteristics," *IEEE Trans. Ind. Electron.*, vol. 67, no. 2, pp. 1555–1567, Feb. 2020.
[4] T. Jiang, J. Zhang, X. Wu, K. Sheng, and Y. Wang, "A bidirectional three-level LLC resonant converter with PWAM control," *IEEE Trans. Power Electron.*, vol. 31, no. 3, pp. 2213–2225, Mar. 2016.
[5] F. Qian, "Research on full-bridge three-level LLC converter based on variable frequency and double phase-shift control," *Guangdong Univ. Technol.*, Guangzhou, China, 2015.
[6] Q. Juan, "Research on digital control full-bridge LLC resonant converter," Nanjing Univ. Aeronaut. Astronaut., Nanjing, China, 2013.
[7] D.-K. Kim, C.-O. Yeon, J.-H. Kim, Y. Jeong, and G.-W. Moon, "LLC resonant converter with high voltage gain using auxiliary LC resonant circuit," in *Proc. 9th Int. Conf. Power Electron. ECCE Asia*, 2015, pp. 1505–1512.
[8] I.-O. Lee, S.-Y. Cho, and G.-W. Moon, "Three-level resonant converter with double LLC resonant tanks for high-input-voltage applications," *IEEE Trans. Ind. Electron.*, vol. 59, no. 9, pp. 3450–3463, Sep. 2012.
[9] B.-G. Chung, K.-H. Yoon, S. Phum, E.-S. Kim, and J.-S. Won, "A novel LLC resonant converter for wide input voltage and load range," in *Proc. 8th Int. Conf. Power Electron.*, Jeju, South Korea, 2011, pp. 2825–2830.
[10] H. Wu, Y. Li, and Y. Xing, "LLC resonant converter with semiactive variable-structure rectifier (SA-VSR) for wide output voltage range application," *IEEE Trans. Power Electron.*, vol. 31, no. 5, pp. 3389–3394, May 2016.
[11] H. Wu, T. Mu, X. Gao, and Y. Xing, "A secondary-side phase-shift-controlled LLC resonant converter with reduced conduction loss at normal operation for hold-up time compensation application," *IEEE Trans. Power Electron.*, vol. 30, no. 10, pp. 5352–5357, Oct. 2015.
[12] D. Fu, F. C. Lee, Y. Liu, and M. Xu, "Novel multi-element resonant converters for front-end dc/dc converters," in *Proc. IEEE Power Electron. Spec. Conf.*, 2008, pp. 250–256.
[13] A. Safaee, P. K. Jain, and A. Bakhshai, "An adaptive ZVS full-bridge DC–DC converter with reduced conduction losses and frequency variation range," *IEEE Trans. Power Electron.*, vol. 30, no. 8, pp. 4107–4118, Aug. 2015.
[14] D. Huang, F. C. Lee, and D. Fu, "Classification and selection methodology for multi-element resonant converters," in *Proc. 26th Annu. IEEE Appl. Power Electron. Conf. Expo.*, 2011, pp. 558–565.
[15] D. Fu, "Topology investigation and system optimization of resonant converters," Ph.D. dissertation, Dept. ECE, Polytechnic Inst. State Univ., Blacksburg, VA, USA, 2010.
[16] T. Mishima, H. Mizutani, and M. Nakaoka, "An LLC resonant full-bridge inverter-link DC-DC converter with an anti-resonant circuit for practical voltage step-up/down regulation," in *Proc. IEEE Energy Convers. Congr. Expo.*, 2012, pp. 3533–3540.
[17] D. Huang, "Investigation of topology and integration for multi-element resonant converters," Ph.D. dissertation, Dept. ECE, Polytechnic Inst. State Univ., Blacksburg, VA, USA, 2013.
[18] D.-K. Kim, S. C. Moon, C.-O. Yeon, and G.-W. Moon, "High efficiency LLC resonant converter with high voltage gain using an auxiliary LC resonant circuit," *IEEE Trans. Power Electron.*, vol. 31, no. 10, pp. 6901–6909, Oct. 2016.
[19] B. Shen, Y. Chen, H. Wang, Y.-F. Liu, and P. C. Sen, "High efficiency wide input voltage range LCLC resonant converter using nonlinear frequency controller," in *Proc. IEEE Energy Convers. Congr. Expo.*, Sep. 2018, pp. 1435–1441.
[20] T. Mishima, H. Mizutani, and M. Nakaoka, "A sensitivity-improved PFM LLC resonant full-bridge DC–DC converter with LC antiresonant circuitry," *IEEE Trans. Power Electron.*, vol. 32, no. 1, pp. 310–324, Jan. 2017.
[21] Q. Zhao, W. Liu, Y. Wang, D. Wang, and N. Wu, "A novel multiresonant DC–DC converter with wide output-voltage range," *IEEE Trans. Power Electron.*, vol. 35, no. 6, pp. 5625–5638, Jun. 2020.

Xiangjun Zhang (Member, IEEE) was born in Shandong Province, China, in 1971. He received the B.S. degree in welding from Xi'an Jiaotong University, Xi'an, China, in 1993, the M.S. degree in welding from the Harbin Welding Institute, Harbin, China, in 1999, and the Ph.D. degree in electrical engineering from the Harbin Institute of Technology, Harbin, China, in 2006.

From 2006 to 2013, he was a Lecturer with the Department of Electrical and Electronics Engineering, Harbin Institute of Technology, where he has been an Associate Professor since 2013. His research interests include the areas of electronic ballast, power factor correction circuits, high-power converters, and light-emitting-diode lighting systems.

Jiachen Jing was born in Heilongjiang Province, China, in 1996. He received the B.S. degree in electrical engineering in 2019 from the Harbin Institute of Technology, Harbin, China, where he is currently working toward the M.S. degree in electrical engineering.

His current research interests focus on high-frequency resonant converters.

Yueshi Guan (Member, IEEE) was born in Heilongjiang Province, China, in 1990. He received the B.S., M.S., and Ph.D. degrees in electrical engineering from the Harbin Institute of Technology (HIT), Harbin, China, in 2013, 2015, and 2019, respectively.

Since 2019, he has been an Associate Professor with the Department of Electrical and Electronics Engineering, HIT. His research interests include areas of high-frequency and very high frequency converters, single-stage ac/dc converter, and high conversion ratio converters.

Mingcong Dai was born in Jilin Province, China, in 1995. He received the B.S. and M.S. degrees in electrical engineering from the Harbin Institute of Technology, Harbin, China, in 2018 and 2020, respectively.

His current research interests focus on high-frequency resonant converters.

Yijie Wang (Senior Member, IEEE) was born in Heilongjiang Province, China, in 1982. He received the B.S., M.S., and Ph.D. degrees in electrical engineering from the Harbin Institute of Technology (HIT), Harbin, China, in 2005, 2007, and 2012, respectively.

From 2012 to 2014, he was a Lecturer with the Department of Electrical and Electronics Engineering, HIT, where he has been an Associate Professor since 2015. His interests include dc–dc converters, soft-switching power converters, power factor correction circuits, digital control electronic ballasts, LED lighting systems.

Dianguo Xu (Fellow, IEEE) was born in Heilongjiang, China, in 1960. He received the B.S. degree in control engineering from Harbin Engineering University, Harbin, China, in 1982, and the M.S. and Ph.D. degrees in electrical engineering from the Harbin Institute of Technology (HIT), Harbin, China, in 1984 and 1989, respectively.

In 1984, he was with the Department of Electrical Engineering, HIT, where he late became a Professor. He then worked as the Dean of the School of Electrical Engineering and Automation from 2000 to 2010, and is currently the Vice President of HIT. His research interests include renewable energy generation technology, power quality mitigation, sensorless vector-controlled motor drives, and high-performance servo system. He has authored or coauthored more than 600 technical papers.

Dr. Xu is an Associate Editor for the IEEE TRANSACTIONS ON INDUSTRIAL ELECTRONICS and the *IEEE Journal of Emerging and Selected Topics in Power Electronics*. He serves as a Chairman of the IEEE Harbin Section.